



MODELLING AND INITIAL ASSESSMENT OF A FUEL CELL AUXILIARY PROPULSION AND POWER UNIT

Moritz G. Kolb¹, Arne Seitz¹, Barlas Türkyilmaz¹, Yiyuan Ma¹, & Mirko Hornung¹

¹Bauhaus Luftfahrt e.V. (BHL), Taufkirchen, Germany

Abstract

The paper discusses the modelling and initial assessment of a novel high-temperature Fuel Cell Auxiliary Propulsion and Power Unit (FC-APPU) for a short-to-medium range multi-fuel passenger aircraft with an entry-into-service of 2035. The FC-APPU is characterized by its ability to not only provide power for aircraft subsystems, but also power for thrust generation. The general system architecture of a FC-APPU is introduced, along with an overview of the implemented cell, stack and system modelling approaches. A baseline aircraft is defined and corresponding profiles for subsystem and propulsive power demands are derived. The fuel cell system is assessed over the entirety of an aircraft mission and integration implications are evaluated in terms of system mass, drag and hydrogen consumption based on different technology scenarios. The results are compared to a Fuel Cell Auxiliary Power Unit (FC-APU) of the same entry-into-service and technology status.

Keywords: high temperature PEMFC, fuel cell propulsion, hydrogen aviation, fuel cell modelling, fuel cell thermal management

1. Introduction

Despite significant technological efforts to improve aircraft fuel efficiency [1], aviation CO₂ emissions have been growing continuously, currently amounting to approximately 3% of global CO₂ emissions [2, 3]. With an estimated rise of 2.4% to 4.1% of Revenue Passenger-Kilometers (RPK) following post-COVID-19 developments predicted by ICAO [4], the goal of reducing aircraft emissions increasingly presents itself as a major aviation industry challenge. Alternative energy sources will play a key role in fighting aircraft emissions in order to achieve the goal of carbon neutrality or even climate neutrality set in Destination 2050 [5] and Waypoint 2050 [6], respectively.

In this context, hydrogen has experienced a great resurgence as an alternative energy source in research and development for achieving net-zero emissions in the aviation sector. Hydrogen not only presents itself as a viable option for combustion in conventional gas turbines, but also allows efficient and NO_x-free power generation through electrochemical conversion in Fuel Cells (FCs). As a result, rapid advancements in FC development have been observed in recent years [7-9]. Nevertheless, further improvements are still to be made to utilize the full potential of FC-based propulsion. In order to make a significant impact on aviation's path to climate neutrality, the applicability of FC technology will need to span from small power demands of a few hundred kilowatts, replacing gas turbine based Auxiliary Power Units (APU) [10, 11], up to serving in the (multi-)megawatt power class for in-flight thrust generation for the major market segments of commercial transport aircraft [12].

However, aside from all the ground-based system transition aspects, transitioning from kerosene to hydrogen will not be an easy task to overcome, as the storage onboard an aircraft will require significant changes in integration and certification. Easing this transition will be a key factor in establishing a new energy source like hydrogen. The European Union-funded Horizon 2022 project HOPE (Hydrogen Optimized Multi-Fuel Propulsion System for Clean and Silent Aircraft) targets to act as a first step in the direction of smoothing such an energy transition in aviation. For this, HOPE aims to combine Ultra-High Bypass Ratio (UHBR) multi-fuel turbofan engines with a Fuel Cell Auxiliary Propulsion and Power Unit (FC-APPU) driving an aft-fuselage Boundary Layer Ingesting (BLI) propulsor [13, 14] (see Figure 1). The goal of this novel propulsion system is to substantially

reduce emissions in a much shorter time horizon than novel aircraft configurations by pursuing a multi-fuel energy approach in a traditional tube-and-wing aircraft configuration with an Entry-Into-Service (EIS) of 2035.

An integral part of the HOPE concept, the FC-APPU, acts on three different levels of aircraft emission reduction. During ground operations, the fuel cell system in combination with the BLI propulsor could be utilized to achieve zero-emission taxiing, improving local air quality in and around airports, while also lowering noise emissions on the community [15]. Diverting power away from the main engines to the fuel cell powered BLI fan also increases the overall aircraft propulsive efficiency in cruise, thereby enabling improved aircraft fuel efficiency [16-18]. Additionally, the FC system may enhance performance characteristics and reduce NO_x emissions of the under-wing engines, in the event that the FC product water can be injected as superheated steam into the engine combustion chamber [19].



Figure 1 – HOPE concept aircraft rendering

In this paper, an initial assessment of both a FC-APU and a FC-APPU of the HOPE project is presented. The primary goal is to assess integration implications in terms of system mass, drag and hydrogen consumption for both Fuel Cell Systems (FCSs) in an EIS 2035 Short-to-Medium Range (SMR) passenger aircraft based on different technology scenarios. At first, as a basis for this paper a baseline aircraft class and mission are defined. This is followed by a fundamental overview of the Proton Exchange Membrane Fuel Cell (PEMFC) technology, which is then applied to the FC-APU and novel FC-APPU configurations. Next, the implemented modelling approaches are introduced. Finally, insightful studies and the corresponding results are presented and discussed.

2. Baseline Aircraft

To assess the impact of both FC-APU and FC-APPU on aircraft performance, a detailed baseline aircraft and corresponding subsystems mission power profile is required. This power demand can then be used to size the FCS in order to ensure that all flight operations can be performed.

For the present paper, an A320- / B737-like class aircraft with an EIS of 2035 and Sustainable Aviation Fuel (SAF) as the energy carrier is selected as the baseline aircraft. The baseline aircraft is derived in Bauhaus Luftfahrt's in-house tool *BLADE* (Bauhaus Luftfahrt Aircraft Design Environment) [20] by considering expected overall aircraft technology improvements and updated Top Level Aircraft Requirements (TLARs) for the desired EIS. In addition, engine improvements up to 2035, including gains in turbomachinery efficiency, increased bypass ratios and updated engine architectures, are derived and estimated in *APSS* (Aircraft Propulsion System Simulation) [21-23].

The final baseline features a design range of 3000 NM with 180 PAX and a design payload of 18000 kg. In cruise, the aircraft operates at Mach 0.78, FL350 and ISA+0K while being powered by two UHBR Geared Turbofan (GTF) engines. Furthermore, the aircraft features an all-electric subsystems architecture. [24]

The corresponding aircraft subsystems mission power profile is derived based on the approach presented by van Wensveen et al. [25], in which the power characteristics are estimated per Air Transport Association (ATA) chapter. In this approach, powers that do not have a significant influence on the total power consumption are estimated by scaling the electrical loads per mission

segment with Maximum Take-Off Mass (MTOM) or the number of Passengers (PAX). For larger power consumers such as the Environmental Control System (ECS, ATA21) and flight controls (ATA27), modified approaches based on Chakraborty [26] and Rao [27] are implemented. For all considered ATA chapters and the corresponding estimation approaches, see Appendix A, Table A. Furthermore, as the aircraft is equipped with an all-electric subsystems architecture, it is necessary to consider engine relight scenarios. The subsystem power required for relighting is derived from the starting power of the General Electric GENx take-off power for the Boeing 787, scaled to maximum engine thrust [28]. This results in two power curves, a maximum subsystems power profile, which both FC-APU and FC-APPU systems must be able to achieve in case of an engine relight case, and a nominal demand profile. Both mission power profiles are shown in Figure 2. Additionally, key aircraft mission operating points are listed in Table 1.

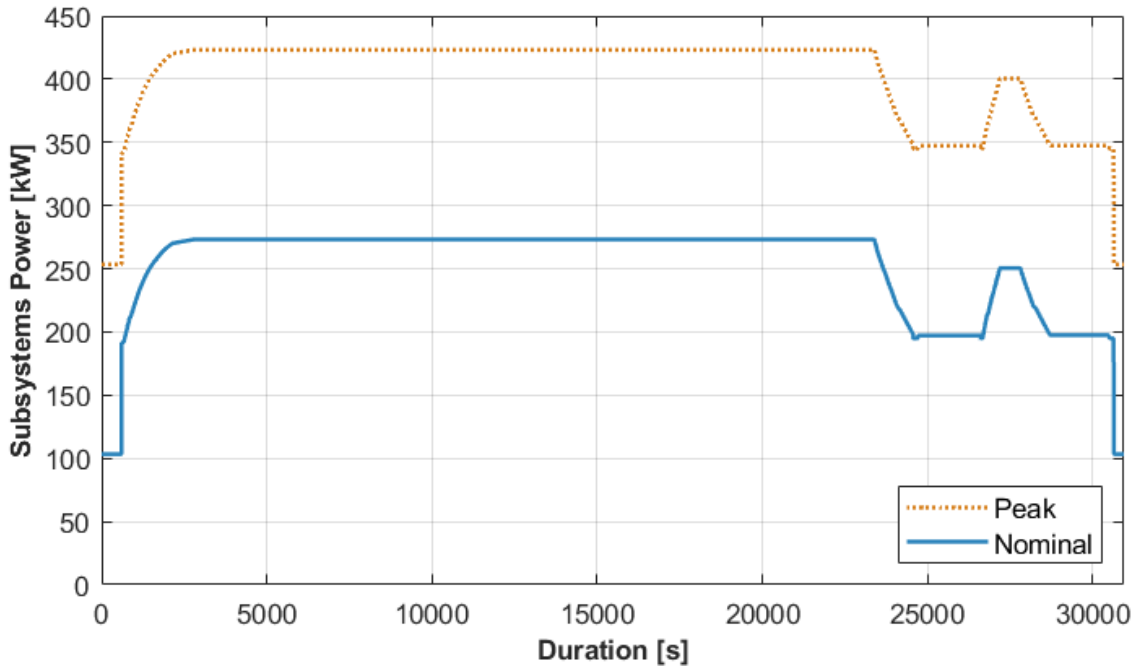


Figure 2 – Baseline aircraft subsystems mission power profiles

Table 1 – Key aircraft mission points

Parameter	Symbol	Unit	Hot-and-High Take-Off (HHTO)	Take-Off (TO)	Top-of- Climb (TOC)	Cruise (CR)
Mach Number	<i>Ma</i>	-	0.2	0.2	0.78	0.78
Altitude	<i>alt</i>	m	1600	0	10668	10668
ISA Deviation	ΔISA	K	+30	+15	+10	0

3. FC-APU and FC-APPU System Architectures

In the context of HOPE, both the FC-APU and the FC-APPU are based on High-Temperature Proton Exchange Membrane Fuel Cells (HT-PEMFCs). Compared to Low-Temperature Proton Exchange Membrane Fuel Cells (LT-PEMFCs), which typically operate at around 60°C to 90°C, HT-PEMFCs cover operating ranges from 120°C to 200°C, with laboratory tested cells even achieving stable operation at temperatures all the way up to 240°C [8, 29, 30]. Compared to LT-PEMFCs, which typically use Perfluorosulfonic Acid (PFSA) polymers as proton-conducting membranes, HT-PEMFCs mostly consist of phosphoric acid-doped membranes such as Phosphoric Acid-doped Benzimidazoles (PA-PBI) [19]. These membranes have the advantage of being proton conductive without external humidification, thus eliminating the need for humidifiers in the FCS. HT-PEMFCs also alleviate Thermal Management System (TMS) requirements as the stack can be operated with

MODELLING AND INITIAL ASSESSMENT OF A FUEL CELL AUXILIARY PROPULSION AND POWER UNIT

higher coolant temperature deltas of up to 100°C [31]. Additionally, the temperature difference to ambient increases, allowing the heat exchanger to be sized smaller and lighter.

In terms of spatial arrangement, the FCSs under consideration are located in the aft of the aircraft fuselage. This is primarily due to space gained by replacing the conventional APU, but also to ensure a close proximity to the LH2 tank, as well as the aft BLI propulsor and thereby reducing fuel system complexity and transmission losses for the FC-APPU case.

The FCSs assessed in this paper are designed to be self-sufficient at all mission flight points, meaning the system must account for FCS specific power requirements (e.g. coolant pump power) on top of the required aircraft subsystem powers. The FCSs in this paper consist of five component domains (see Figure 3): the fuel cell stack, the anode stream components, the cathode stream components, the TMS and the electrical power components. The fuel cell stack contains the individual cells and is the core component of the FCS and interacts with all other system sections.

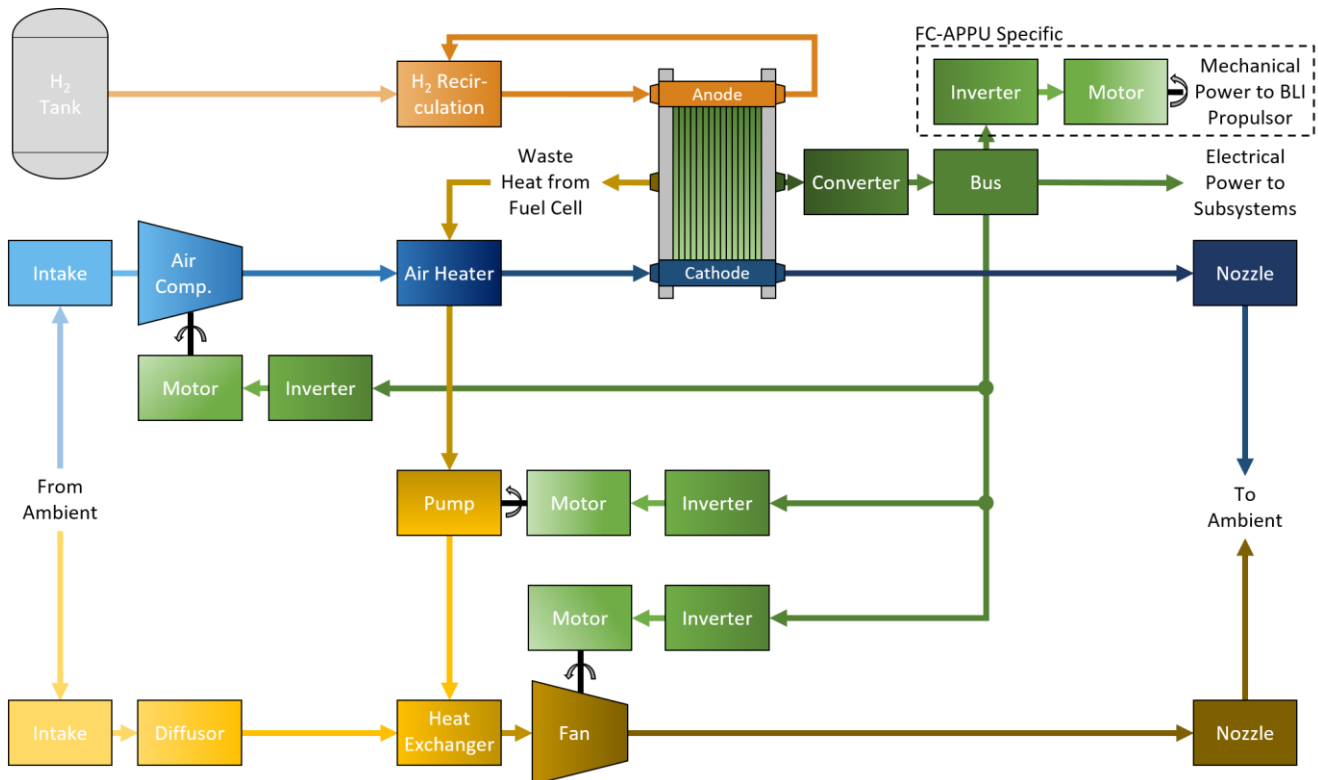


Figure 3 – FC-APU and FC-APPU system architecture

For this assessment, the anode stream is represented only just before entering the FCS. Therefore, hydrogen tanks, heating and pressurization are not considered for the time being. However, it is legitimately conceivable that hydrogen heating can be achieved by using aircraft heat sinks, such as electrical component cooling or the ECS. In addition, as the stack typically operates at stoichiometric conditions of greater than one, an anode recirculation is implemented in order to minimize hydrogen consumption.

The cathode air is drawn directly from ambient and is pressurized by an air compressor located after the air intake. The air stream is also preheated by passing the stack heat through an air heater just before entering the cathode. The remaining air exiting the cathode is expanded to ambient conditions through a nozzle.

As the fuel cell stacks generate a significant amount of waste heat, a TMS is required to maintain the operating temperature within a desired range. In the present case, the TMS is implemented in the form of a ram-air heat exchanger arrangement, which allows a detailed estimation of the TMS mass, but also the drag resulting from stack heat removal. The ram-air TMS consists of a compact cross-flow heat exchanger to dissipate heat to the environment, a diffusor to reduce the cooling air velocity, a nozzle to recover the cooling air momentum, a pump to recover the coolant pressure losses and pipes for coolant transfer. In case the cooling airflow needs to be increased (e.g. during take-off), a fan can be activated as well. [32]

The final component section includes the Power Management and Distribution (PMAD) system and the electrical machines of the FCS. The PMAD serves to connect all electrically driven components to the fuel cell power output. This includes FCS specific powers for the cathode stream compressor, the TMS coolant pump and fan, as well as aircraft specific subsystem powers. In addition, for FC-APPU systems, the power demand is further extended by the electric motors for mechanical power generation required to drive the BLI propulsor in the aft of the aircraft.

4. Methodology

The fuel cell system architectures assessed in this paper are modelled in the newly developed Bauhaus Luftfahrt in-house tool *HyPE* (Hybrid Propulsion Environment). *HyPE* is a steady-state simulation framework for hybrid(-electric) propulsion architectures based on the multidisciplinary analysis and optimization package *OpenMDAO* [33]. In the following subchapters, the fuel cell system modelling approaches implemented in *HyPE* are presented following a bottom-up approach, starting at the cell level and migrating to the stack and then to the complete system level (see Figure 3).

4.1 Cell Modelling

An analytical pressure and temperature dependent polarization curve modelling approach has been implemented to fully assess different cell operating conditions throughout an entire aircraft mission. The cell voltage U_{cell} is calculated with the occurring cell voltage losses:

$$U_{cell} = U_{nernst} - U_{act} - U_{ohm} - U_{conc} \quad (1)$$

With U_{nernst} as the reversible or no-loss cell voltage and U_{act} , U_{ohm} and U_{conc} as the fuel cell voltage losses, taking into account activation and crossover losses, ohmic losses and concentration losses, respectively (see a cell voltage example in Figure 4).

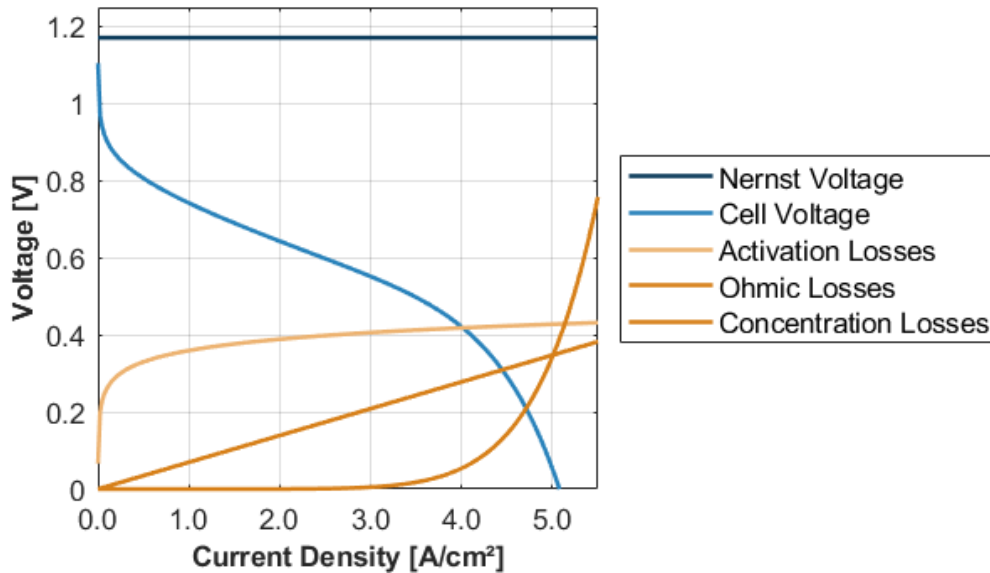


Figure 4 – Fuel cell polarization curve example

The reversible cell voltage, also known to as the Nernst voltage, is based on the Gibbs free energy, which is affected by the fuel cell pressure and the concentration of the reactants [34].

$$U_{nernst} = E_0 + \frac{R \cdot T}{2 \cdot F} \cdot \ln \left(\frac{a_{H_2} \cdot a_{O_2}^{0.5}}{a_{H_2O}} \right) \quad (2)$$

Where E_0 is the cell Electromotive Force (EMF) at standard pressure, R is the universal gas constant, T is the operating temperature, F is the Faraday constant and a is the activity of hydrogen (H_2), oxygen (O_2) and water (H_2O).

MODELLING AND INITIAL ASSESSMENT OF A FUEL CELL AUXILIARY PROPULSION AND POWER UNIT

Activation and crossover losses dominate at low current densities of the polarization curve and are caused by the slowness of the reaction on the surface of the electrodes as well as losses due to fuel waste passing through the electrodes [34]. It is defined as:

$$U_{act} = \frac{R \cdot T}{2 \cdot \alpha \cdot F} \cdot \ln \left(\frac{i + i_n}{i_0} \right) \quad (3)$$

Where α is the charge transfer coefficient, i is the cell load current density, i_n is the internal current density and i_0 is the exchange current density.

The exchange current density defines the ability of a catalyst to facilitate an electrochemical reaction and can be calculated as introduced by Newman [35]:

$$i_0 = i_{0,ref} \cdot \left(\frac{p_{O_2}}{p_{O_2,ref}} \right)^\gamma \cdot e^{\left(\frac{-E_c}{R \cdot T} \left(1 - \frac{T}{T_{ref}} \right) \right)} \quad (4)$$

The exchange current density at any oxygen partial pressure p_{O_2} and temperature T can be related to a reference exchange current density $i_{0,ref}$ at a specific reference oxygen partial pressure $p_{O_2,ref}$ (101325 Pa) and reference temperature T_{ref} (353.15 K) with γ as the kinetic reaction order and E_c as the activation energy of the oxygen reduction reaction.

The ohmic voltage losses U_{ohm} mainly occur due to the ionic resistance in the electrolyte and can be expressed with the thickness of the electrolyte layer δ_{thick} and the electrolyte conductivity σ [36]:

$$U_{ohm} = i \cdot \frac{\delta_{thick}}{\sigma} \quad (5)$$

Finally, at high current densities, concentration voltage losses U_{conc} increasingly contribute to the voltage drop in the polarization curve. Concentration losses occur as a result of a change in reactant concentration at the surface of the electrodes as the fuel is being used, meaning the fuel cell consumes more reactants than it can supply to the electrodes [36]. U_{conc} is defined as:

$$U_{conc} = \frac{R \cdot T}{2 \cdot F} \cdot \ln \left(\frac{i_{lim}}{i_{lim} - i} \right) \quad (6)$$

It is limited by the limiting cell current density i_{lim} , the largest sustainable current density that can be passed through the FC electrolyte.

Based on the fuel cell reaction, the air and hydrogen consumption can be calculated from the cell power P_{cell} , the cell voltage V_{cell} , and the molar masses of air and hydrogen, M_{air} and M_{H_2} , respectively:

$$w_{air} = \frac{M_{air} \cdot P_{cell}}{\varphi_{O_2} \cdot 4 \cdot V_{cell} \cdot F} \quad (7)$$

$$w_{H_2} = \frac{M_{H_2} \cdot P_{cell}}{2 \cdot V_{cell} \cdot F} \quad (8)$$

The heat Q_{cell} produced by the cell during FC operation is derived from the ideal cell voltage $V_{ideal,LHV}$ with respect to the lower heating value of hydrogen.

$$Q_{cell} = P_{cell} \cdot \left(\frac{V_{ideal,LHV}}{V_{cell}} - 1 \right) \quad (9)$$

With this approach, polarization curves can be fitted to any FC specification based on sufficient data and the previously described formulas. Once fitted, the implemented approach also allows for adjustments and studies that extend the original FC data. For example, cell characteristics such as the electrolyte layer thickness or operating pressures can be varied in order to assess possible future technological implications.

4.2 Stack Modelling

Based on the cell operating characteristics, the stack is sized to meet the desired power requirements set in the FCS while staying within a maximum stack voltage U_{stack} or a maximum stack amperage I_{stack} . Depending on where the design operating point of the FC is set on the polarization curve, either U_{stack} or I_{stack} limit the amount of cells connected in parallel or in series. The number of parallel and serial cells are defined as follows:

$$N_{ser} = \frac{U_{stack}}{U_{cell}} \quad (10)$$

$$N_{par} = \frac{I_{stack}}{I_{cell}} = \frac{I_{stack}}{i \cdot A_{cell}} \quad (11)$$

Where the cell current I_{cell} is calculated from the current density i and the cell area A_{cell} . Combining the serial and parallel number of cells yields the total cell count. Cell outputs, such as the required air and hydrogen mass flows, are scaled to the stack level based on the total cell count.

For each mission point, the hydrogen mass flow required to operate the FCS at the given output power is calculated. This value is then multiplied by the mission point duration resulting from the baseline aircraft mission defined in Section 0. Adding up all the mission points leads to the total mission fuel mass of the FCS.

In terms of estimating the mass of the FC stack, the mass can be estimated either based on cell count or maximum power, with an individual cell mass or a defined specific power with reference to the maximum installed stack power.

The FC stack can also be oversized, meaning the maximum installed stack power is higher than the required. Oversizing shifts the design point of the fuel cell to lower current densities and therefore higher voltages. Oversizing is defined by the oversizing factor OF :

$$OF = \frac{P_{max}}{P_{req}} \quad (12)$$

It is defined as the ratio of maximum installed stack power P_{max} and the required stack power P_{req} .

4.3 System Modelling

Lastly, the FC stack must be integrated into the overall FCS. In order to fully evaluate the FCSs described in Section 3 of this paper, the cathode gas stream, the TMS and the electrical components must be modelled. The following subsections describe these FCS subsystems in more detail.

4.3.1 Cathode Gas Stream

Following the airflow into the FCS system, the cathode stream is extracted directly from ambient. Ambient conditions are calculated based on the ICAO standard atmosphere [37] with the flight conditions acting as inputs.

The air is passed through an intake that calculates the total temperature and pressure as a result of static flight conditions and a defined intake pressure ratio PR_{in} .

$$T_t = T_s \cdot \left(1 + Ma^2 \cdot \frac{\gamma-1}{2}\right) \quad (13)$$

$$p_t = p_s \cdot \left(1 + Ma^2 \cdot \left(\frac{\gamma-1}{2}\right)^{\frac{\gamma}{\gamma-1}}\right) \cdot PR_{in} \quad (14)$$

Since the air requires compression to the desired operating pressure, a simple compressor model is implemented to account for the pressurization power, air temperature rise and compressor mass.

$$P_{cmp} = \frac{1}{\eta} \cdot w_{in} \cdot c_p \cdot T_{in} \cdot \left(\frac{p_{out}}{p_{in}}\right)^{\left(\frac{\gamma-1}{\gamma}-1\right)} \quad (15)$$

$$T_{out} = T_{in} \cdot \left(1 + \frac{1}{\eta}\right) \cdot \left(\frac{p_{out}}{p_{in}}\right)^{\left(\frac{\gamma-1}{\gamma}\right)} \quad (16)$$

The compression power P_{cmp} and the compressor outlet temperature T_{out} are estimated via isentropic relations with w_{in} as the mass flow, c_p as the specific heat capacity, T_{in} as the inlet temperature, η as the compressor efficiency, γ as the heat capacity ratio and p_{in} and p_{out} as the inlet and outlet pressures of the compressor.

The mass of the compressor is estimated by a correlation based on the results of Tornabene et al. [38]. The compressor mass m_{cmp} is correlated with the inlet pressure p_{in} and outlet pressure p_{out} and the mass flow w_{in} into the compressor. The correlation is defined as follows:

$$m_{cmp} = -0.05 \cdot \left(\frac{p_{out}}{p_{in}}\right)^3 + 0.8 \cdot \left(\frac{p_{out}}{p_{in}}\right)^2 - 4.82 \cdot \left(\frac{p_{out}}{p_{in}}\right) + 19.87 + 8.549 \cdot (w_{in} - 1.16) \quad (17)$$

Although the temperature is increased by compression, HT-PEMFC operating conditions require an additional heating component to bring the incoming cathode air to operating temperatures. Since the cooling flow is routed across the cathode airflow, it is assumed that the remaining temperature delta for a stable operation is achieved by the hot side coolant outlet flow of the FC stack. This results in a reduced heat removal for the TMS.

4.3.2 Thermal Management System

The ram-air based TMS used in this paper consists of an intake, a diffuser, a compact heat exchanger, an optional puller fan and a nozzle for the cold side air. For the coolant hot side, necessary piping assemblies including a pump for pressurizing the coolant are considered (see Figure 3 in Section 3). The TMS is modelled in *ICCE* (Innovative Cooling Concept Environment), a Bauhaus Luftfahrt in-house modelling framework for TMSs based on steady-state fluid simulation [39]. The ram-air TMS setup and the implemented methods are described in detail by Kellermann et al. [32]. In summary, this approach allows a complete analysis of the required TMS power, stream tube drag and mass for the FCS design.

In addition, the TMS is designed to remove excess heat from the FC stack at each mission point. In return, the stack must provide sufficient power via the PMAD for the TMS pump and puller fan.

4.3.3 Power Management and Distribution System and Electrical Machines

The PMAD system of the FCS connects all electrical loads in the system, while the electrical machines provide power to mechanical consumers (e.g. the cathode compressor). PMAD components include converters, cables and inverters. All of these electrical components, including the electrical motors, are modelled at a low fidelity level by considering only their electrical efficiencies η_{elec} .

$$P_{out} = P_{in} \cdot \eta_{elec} \quad (18)$$

$$Q_{elec} = P_{in} - P_{out} \quad (19)$$

Where P_{out} is the electrical or mechanical output power of the power system component, P_{in} is the input power and Q_{elec} is the heat generated.

The mass of the PMAD components and electric machines m_{pow} is estimated by applying the specific power q_{pow} to the maximum power demand P_{max} over the entire aircraft mission.

$$m_{pow} = P_{max} \cdot q_{pow} \quad (20)$$

Compared to converters, inverters and motors, cable masses are calculated with the specific meter mass q_{cab} based on cable length l_{cab} and not on maximum power.

$$m_{cab} = l_{cab} \cdot q_{cab} \quad (21)$$

5. Studies

For the initial assessment of the FC-APU and FC-APPU performed in this paper, each system is analyzed on three different levels. At the cell level, the effect of varying operating pressure is evaluated. For the stack, different oversizing approaches are considered and at the FCS level, different TMS sizing conditions are assessed. The objective of these assessments is to provide an initial estimate for best-and-balanced overall FCS designs capable of providing sufficient subsystem and mechanical power to enable operation with minimal drawbacks along the entire baseline aircraft mission.

Additionally, given the inherent unpredictability of technological advancements, three technology scenarios for a target EIS of 2035 for the FC stack are addressed: standard (STD), intermediate (INT) and optimistic (OPT). Each successive step in these scenarios represents a more radical technology improvement for the year 2035.

The FC technology scenarios presented in this paper are centered around the promising technology of HT-PEMFCs. Although the FCSs in this paper are HT-PEMFC driven, based on the EIS of 2035, it is initially assumed that HT-PEMFCs will achieve similar operating characteristics as currently available LT-PEMFCs. Therefore, polarization curve behaviors based on state-of-the-art LT-PEMFCs [40] are adopted for this evaluation. The polarization curves for different operating pressures are shown in Figure 5. Key fuel cell operating parameters are provided in Table 2.

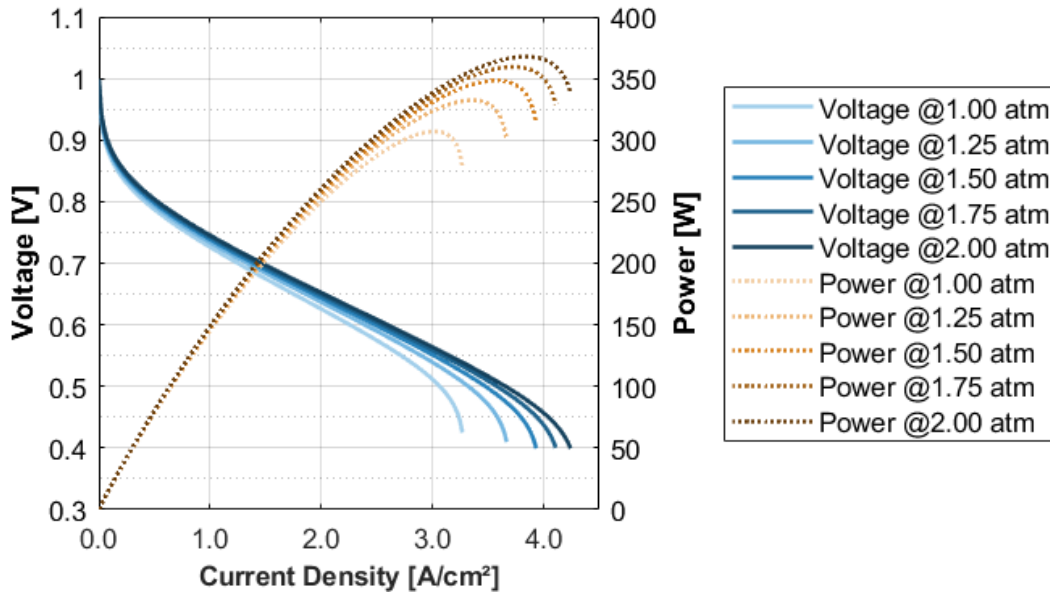


Figure 5 – Cell polarization and power curves

Table 2 – Fuel cell operating data

Fuel Cell Parameter	Symbol	Unit	Value
Operating Temperature	T_{op}	°C	160
Operating Pressure	p_{op}	atm	1.0 – 2.0
Maximum Stack Voltage	$U_{stack,max}$	V	1000
Anode Stoichiometry	λ_{an}	-	1.5
Cathode Stoichiometry	λ_{cat}	-	2.0

For the FCS, general efficiency and specific power assumptions are made to assess realistic transmission losses and masses of the air stream and electrical components (see Figure 3), which are presented in Table 3. To determine the impact of the FC stack sizing and operational inputs, the technology scenario variation affects only the stack specific power. This variation is shown in Table 4 and is in compliance with technology development predictions for HT-PEMFCs (see [41, 42]). It is important to note that during stack mass estimation, the stack specific power is always applied to the

MODELLING AND INITIAL ASSESSMENT OF A FUEL CELL AUXILIARY PROPULSION AND POWER UNIT

maximum possible stack output power (i.e., maximum power output at maximum operating pressure).

Table 3 – FCS component assumptions

FCS Parameter	Symbol	Unit	Value
Intake Pressure Ratio	PR_{in}	-	0.990
Compressor Efficiency	η_{cmp}	-	0.850
Motor Efficiency	η_{mot}	-	0.980
Motor Specific Power	q_{mot}	kW/kg	17.5*
Inverter Efficiency	η_{inv}	-	0.990
Inverter Specific Power	q_{inv}	kW/kg	17.5*
Cable Efficiency	η_{cab}	-	0.995
Cable Meter Mass	q_{cab}	kg/m	5.0*
Cable Length	l_{cab}	m	5.0*
Converter Efficiency	η_{conv}	-	0.985
Converter Specific Power	q_{conv}	kW/kg	7.5*

*derived from [43] and [44]

Table 4 – Stack specific power technology scenario variation

Scenario	Symbol	Unit	Value
Standard (STD)	$q_{stack,STD}$	kW/kg	3.0
Intermediate (INT)	$q_{stack,INT}$	kW/kg	6.0
Optimistic (OPT)	$q_{stack,OPT}$	kW/kg	10.0

Ram-air based TMS and heat exchangers in particular possess a high potential for optimization as shown by Kellermann et al. [32]. However, for the purpose of the present studies and in order to better assess FC stack sensitivities, heat exchanger parameters are kept constant and are set to an initial best guess. Key parameter assumptions for the compact cross-flow heat exchanger are listed in Table 5.

Table 5 – Heat exchanger parameter assumptions

Heat Exchanger Parameter	Symbol	Unit	Value
Cold Side Hydraulic Diameter	$d_{h,c}$	mm	5.0
Hot Side Hydraulic Diameter	$d_{h,h}$	mm	0.5
Cold Side Pressure Ratio	PR_c	-	0.95
Hot Side Pressure Ratio	PR_h	-	0.98
Ratio of Heat Capacities (C_c/C_h)	C_R	-	0.75
Wall Thickness	d_w	mm	1.0

As the stack operates at temperatures higher than 100°C, water is not sufficient as a coolant. Therefore, Dynalene HC-50, a potassium formate- / water-based heat transfer fluid, was chosen for the present studies. HC-50 exhibits a high operating temperature range, spanning from -50°C to 210°C, suitable for use in closed systems [45]. Its integration into the TMS modelling in *ICCE* is facilitated by the thermophysical property library *CoolProp* [46].

For the FC-APPU, a required BLI fan disc power of 3.0 MW was determined by Battiston et al. [47] based on the previously defined baseline aircraft and with the optimality approach for propulsive fuselages introduced by Seitz et al. [16, 48]. It should be noted that, as a preliminary estimation of the FC-APPU system, the required fan disc power is set constant for all mission points and all assessments conducted in this paper.

To account for potential system failures, each stack is designed to have an additional 25% of excess power on top of the required peak power (i.e., a $OF = 1.25$). This ensures that, in the event of cell

failures, the system can still maintain stable operation. Furthermore, the operating temperature, pressure, stoichiometry and maximum stack voltage are kept constant throughout the entire mission. If not specified otherwise, a standard (STD) technology scenario for the FC mass estimation is assumed.

5.1 Operating Pressure Study

For the analysis on cell level, the operating stack pressure is varied from 1.0 to 2.0 atm for both the FC-APU and FC-APPU. Initially, the sizing critical points of the FCSs are identified based on the entire baseline aircraft mission. For both systems, Top-of-Climb (TOC) represents the sizing critical point for the stack, cathode stream and electrical components. This is primarily due to the fact that the air stream into the FC has to be pressurized significantly higher because of the lower ambient pressure at high altitudes. This is especially true for high operating pressures (see Figure 6). In contrast, for the TMS, Hot-and-High Take-Off (HHTO) is crucial for sizing due to the reduced temperature difference between the stack operating temperature and the hot ambient conditions in 1600 m at ISA+30K (see Table 1).

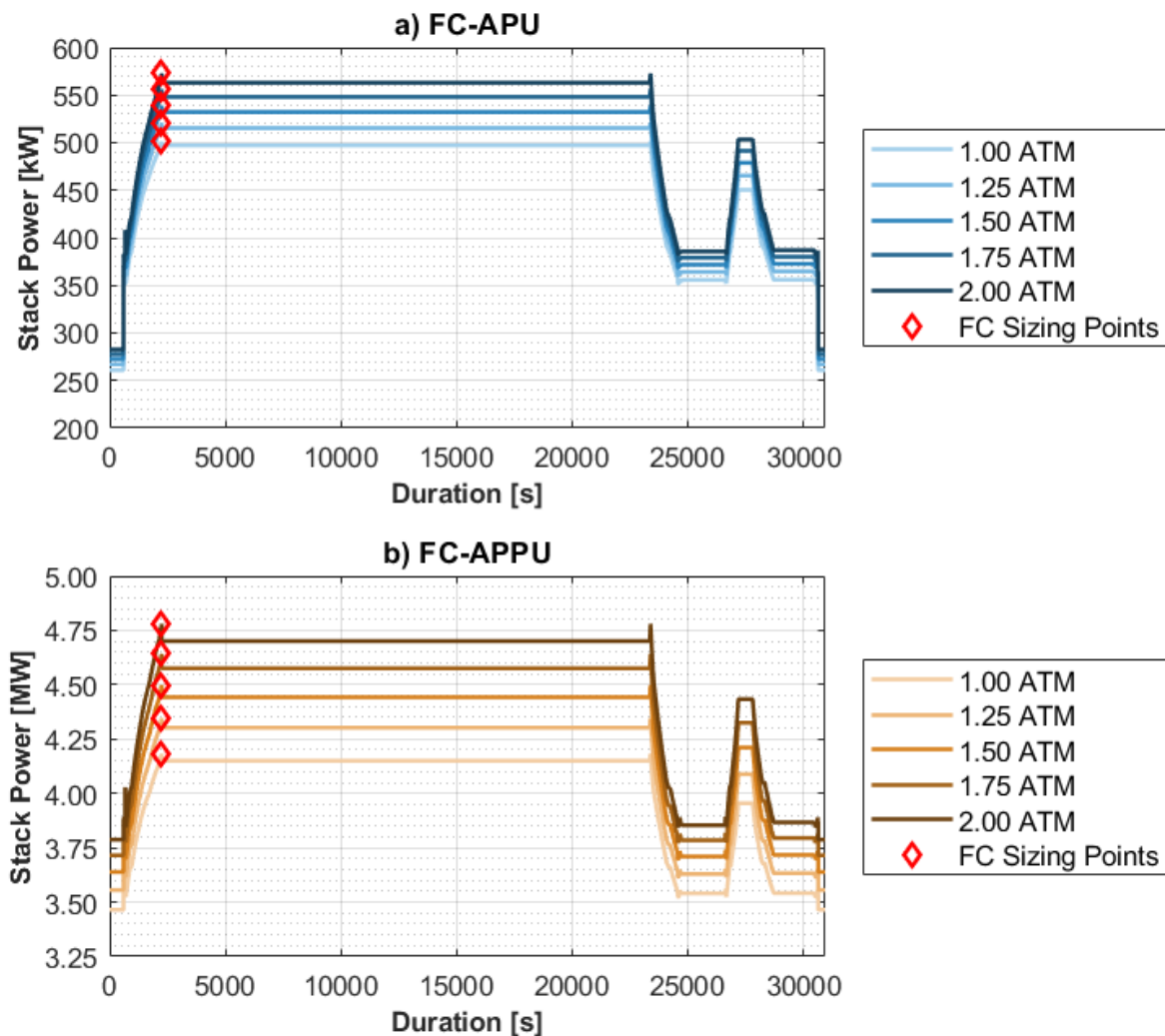


Figure 6 – FC-APU (a) and FC-APPU (b) power and FC sizing points for different operating pressures

As the operating pressure increases, the mass of the FCS, mission fuel mass and TMS drag (i.e., heat to be removed) increase for both FCSs (see Figure 7). In contrast, lower operating pressures benefit from less compressor power for the cathode gas stream, as the pressure delta between ambient conditions and stack conditions reduces. Consequently, less overall stack power is required, leading to a reduction in fuel consumption and less heat being produced by the stack, which in turn leads to lighter TMSs with less drag.

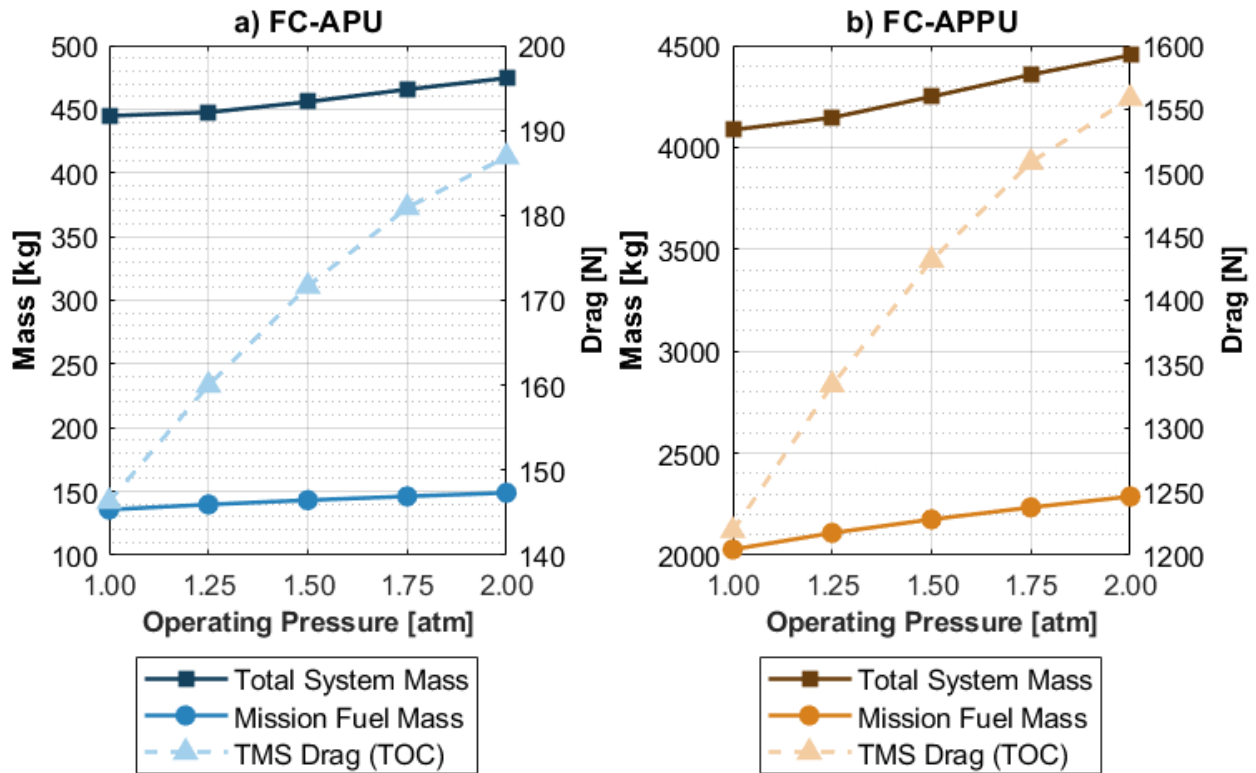


Figure 7 – FC-APU (a) and FC-APPU (b) total system mass, mission fuel mass and TMS drag

For both systems, drag increases by almost 28% between 1.0 and 2.0 atm operating pressure. This increase is primarily rooted in the fact that for an increased heat removal, the compact heat exchanger stack height has to increase in order to achieve the required coolant outlet temperature. This leads to a larger heat exchanger inlet area and therefore an increased TMS drag. For the total system mass (i.e., all components defined in Figure 3), the FC-APU increases by 7% and for the FC-APPU by 9%, respectively. A 10% increase for the FC-APU and 13% for the FC-APPU can be observed for the mission fuel mass. Both the system mass and fuel mass increase more for the FC-APPU due to greater stack power increases for higher pressures (see Figure 6).

5.2 Oversizing Study

If a FCS is oversized, the design and operating points are shifted to lower current densities on the polarization curve, resulting in higher operating efficiencies and lower stack heat. This leads to a reduction in fuel flow as well as TMS mass and drag, which are of course beneficial aspects for aircraft integration. However, oversized also leads to a heavier stack. Both FCS are evaluated within a range of $OF = 1.25$ to 2.5 . The corresponding results are depicted in Figure 8.

The total system mass of both FCSs increases with increasing operating pressure, reaching up to 46% for 1.0 atm and 25% for 2.0 atm with increasing oversizing factors. In contrast, the fuel mission mass and TMS drag exhibit a reversed trend, with fuel decreasing up to 17.5% and drag decreasing up to 46.5% for high oversizing factors. Therefore, oversized represents a trade-off between increasing the total system mass and improving the efficiency of the stack (i.e., reduced hydrogen consumption and TMS drag). This reversed trend illustrates the potential for optimization on an aircraft integrated level, where an optimal balance between operating pressure and oversizing factor can be obtained.

In addition, a local minimum for the total system mass of both FCS architectures occurs at high oversizing factors for operating pressures between 1.25 and 1.50 atm. This optimum is attributed to the manner in which the mass of the stack is estimated. As previously described at the beginning of Section 5, the stack mass is always applied to the maximum stack power at the maximum possible operating pressure (i.e., 2.0 atm), despite possibly operating at a lower pressure. As the degree of oversizing increases, the design points on the power curves move to lower current densities (see

MODELLING AND INITIAL ASSESSMENT OF A FUEL CELL AUXILIARY PROPULSION AND POWER UNIT

Figure 5), thereby increasing the difference between the design cell power and the maximum achievable cell power for lower operating pressures. Consequently, the required stack mass increases more for low operating pressures at higher oversizing, which in turn results in the optimum total system mass moving to higher operating pressures.

If the pressure dependent polarization curves of the cell were to be father spread apart, the above described trends for the total system mass, fuel consumption and TMS drag would be increasingly steeper due to larger differences in cell efficiencies.

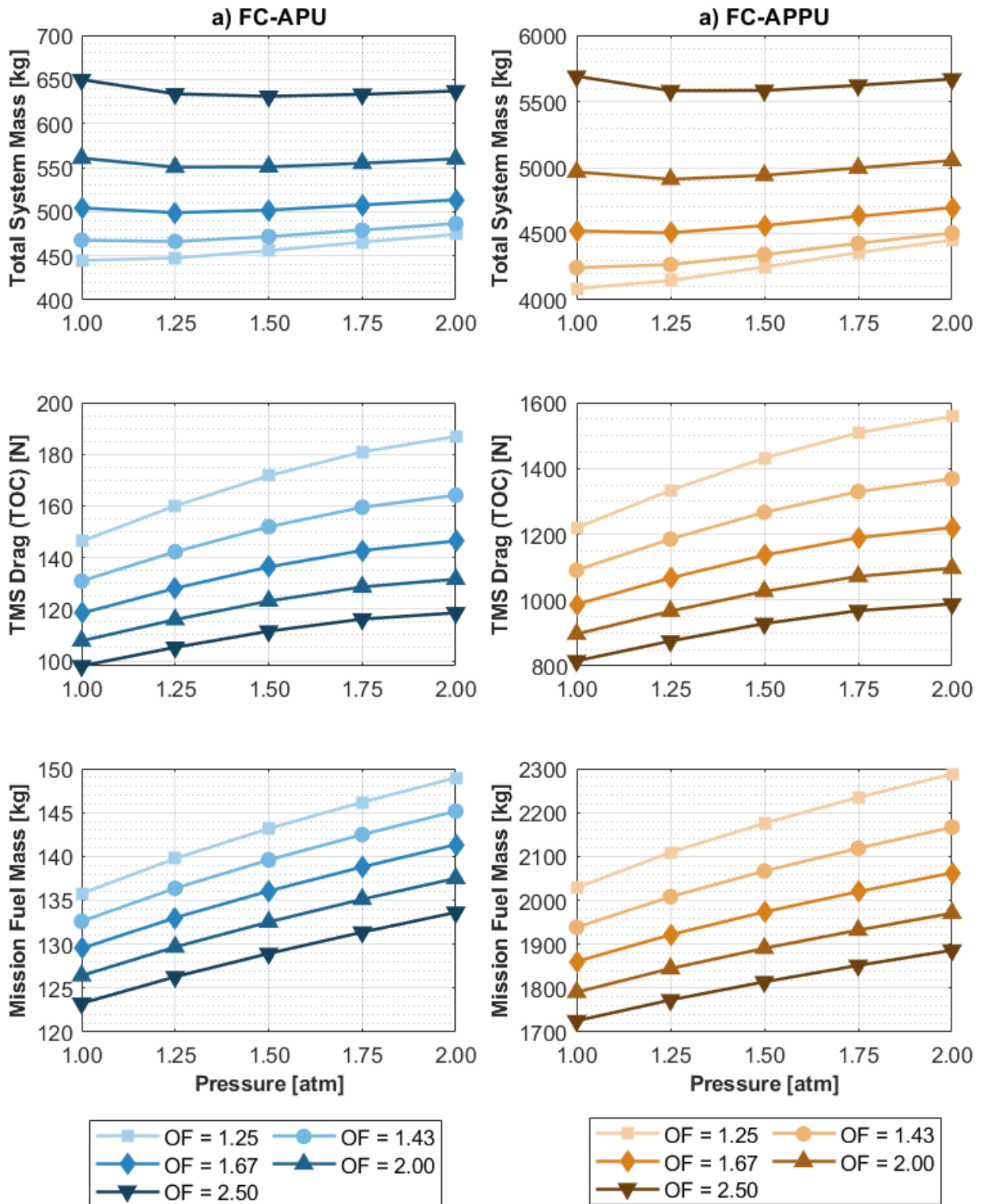


Figure 8 – FC-APU (a) and FC-APPU (b) total system mass, mission fuel mass and TMS drag for varying pressures and oversizing factors

5.3 Technological Scenario Study

In terms of technological advancements until the EIS of 2035, especially the impact of fuel cell stack mass will play an important role for the aircraft integration of the FC-APU and FC-APPU system in the HOPE project. Consequently, the previously conducted studies on operating pressure and oversizing factor were therefore also carried out on the technology scenarios defined at the beginning of Section 5, with a special focus on total system mass. The results of the technology scenario variation with an *OF* of 1.25 (solid line) and 2.5 (dashed line) are presented in Figure 9.

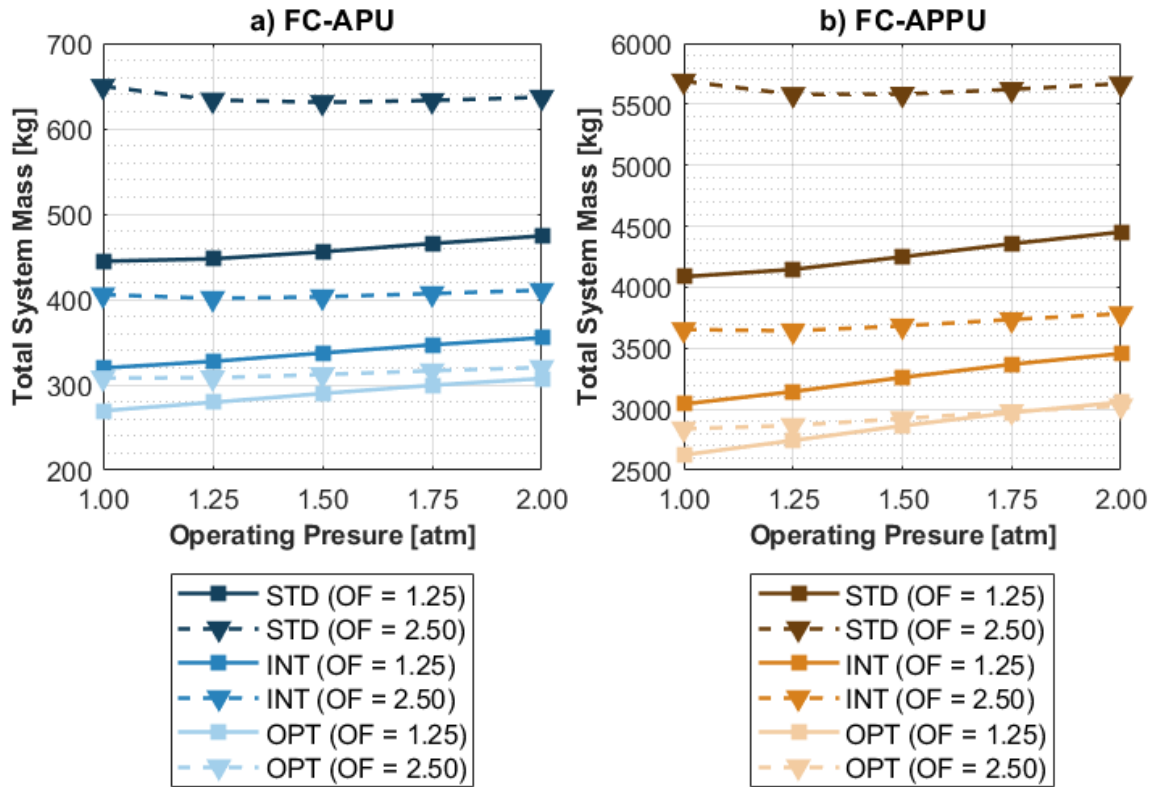


Figure 9 – FC-APU (a) and FC-APPU (b) technology scenario assessment

The results observed in Section 5.2 are replicated here, with the identification of a local optimum between operating pressures of 1.25 and 1.50 atm for high oversizing factors in a standard technology scenario.

In both system configurations, the lowest system mass is achieved with the lowest FC operating pressure and smallest oversizing. However, with greater technology advancements (i.e., lower fuel cell stack masses), the deltas for oversizing become increasingly smaller. This is primarily due to the fact that for a lighter stack, the remaining system masses (TMS and PMAD) begin to have a greater impact on the overall system masses. For the FC-APPU, operating at pressures above 1.75 atm and with an optimistic technology scenario, this effect is so pronounced that a system with an *OF* of 2.5 is as light as the system with an *OF* of 1.25. To better illustrate the impact of mass, the component mass distribution for both systems at an operating pressure of 1.75 atm is depicted in Figure 10.

The mass of the FC stack increases in proportion to the oversizing factor. The masses of the electrical components and cathode stream compressor remain constant across the variations of operating pressure, oversizing and technology scenario, as the required power and component efficiencies also remain consistent for all cases. The mass of the TMS decreases by approximately one-third in a linear fashion in response to the decreased heat output resulting from stack oversizing (i.e., higher cell efficiencies).

Similar to the results of the oversizing study in Section 5.2, counteracting trends are expected for the overall system mass compared to fuel consumption and TMS drag. As the total system masses for oversizing factors with higher technology advancements move closer together, optimal FCS operating conditions and stack oversizing will most likely change. Therefore, defining a well-rounded

stack mass assumption will be crucial for future assessments.

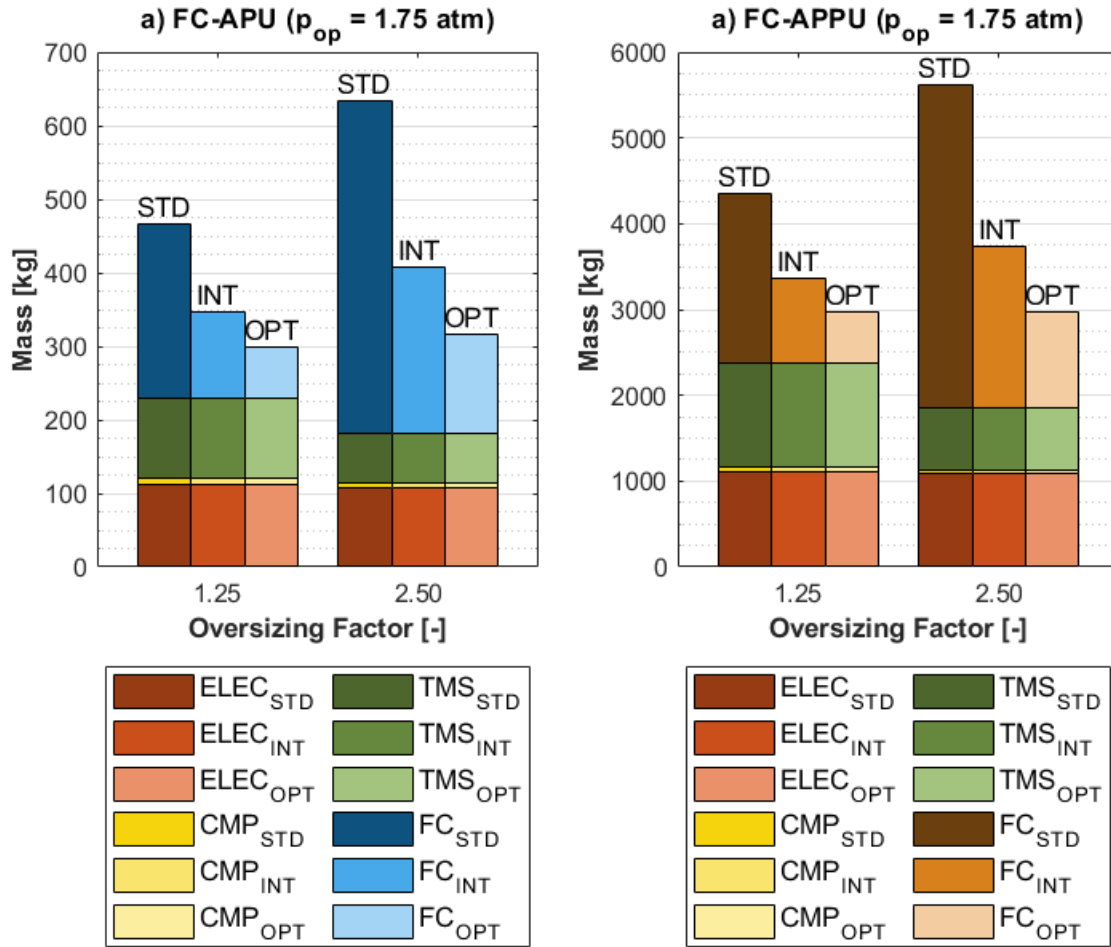


Figure 10 – FC-APU (a) and FC-APPU (b) system mass distribution at 1.75 atm operating pressure

5.4 TMS Study

Another valuable lever for affecting the overall system mass and drag are the FC stack cooling requirements and limits. For the previous studies, an operating temperature of 160°C and a coolant temperature delta of 60°C were assumed as a baseline. However, depending on future technology advancements, higher operating temperatures and coolant deltas may become more feasible [8, 29, 30]. Consequently, an independent investigation was conducted on the TMS to assess the impact of these inputs. This involved examining the influence of varying coolant inlet and exit temperatures, while maintaining a constant stack heat (see Table 6). The stack heat applied in this study represents the heat produced by a FC-APPU architecture with an operating pressure of 1.0 atm and an oversizing factor of 1.25.

Table 6 – TMS study settings

TMS Parameter	Symbol	Unit	Range
Coolant Inlet Temperature	$T_{cool,in}$	°C	120 – 200
Coolant Outlet Temperature	$T_{cool,out}$	°C	60 – 140
Stack Heat	Q_{stack}	MW	3.93

The lowest masses are achieved with increasingly larger temperature differences between the inlet and outlet of the coolant. As the inlet temperature of the coolant increases, the flow lengths of both the hot side (coolant) and cold side (air) of the compact heat exchanger (see “Heat Exchanger” in Figure 3) increase, as more flow length is needed to achieve the desired outlet temperature. Concurrently, the height of the heat exchanger increases as the inlet temperature falls, requiring

additional stacks of hot and cold side channels to achieve the desired heat removal. As a result, an optimum for the TMS mass is formed for temperature differences of 60°C between the coolant inlet and outlet (see Figure 11, left side).

Higher temperature deltas lead to a higher compact heat exchanger effectiveness, resulting in a hotter air exit temperature and therefore less stream tube drag (see Figure 11, right side). For an inlet temperature of 200°C and an outlet temperature of 60°C the TMS can even achieve a slightly positive net thrust.

The degree of temperature difference the FC stack can withstand and the minimum operating temperature required for a stable operation are key factors in determining the best-and-balanced FCS configuration for aircraft integration. Furthermore, modifying and optimizing the specified heat exchanger assumptions presented in Table 5 could result in additional reductions in TMS mass and drag.

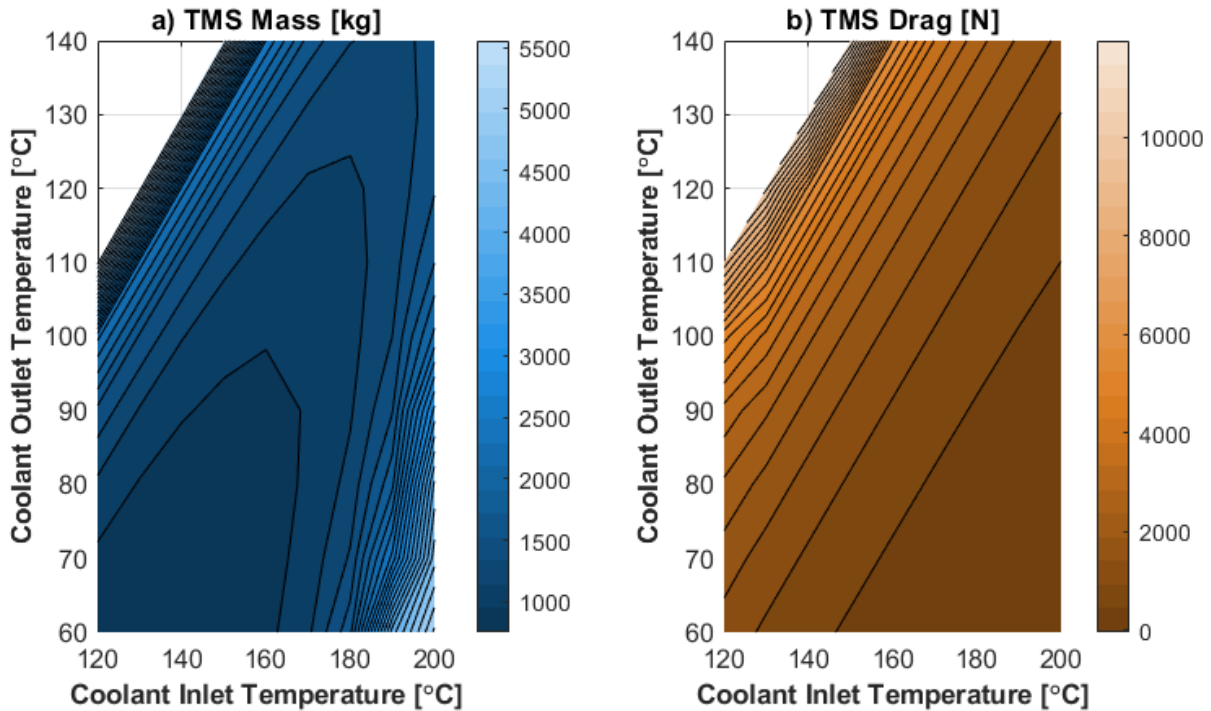


Figure 11 – TMS mass (a) and TMS drag (b) for varying coolant temperatures

6. Conclusion and Outlook

In the present paper, HT-PEMFC based FC-APU and FC-APPU system concepts were introduced and initially assessed. Both systems were analyzed based on a defined baseline aircraft mission, taking into account varying flight conditions and subsystems powers.

Consistent analytical modelling approaches for the cell, stack and system levels were developed and implemented in *HyPE*, a newly developed steady-state hybrid(-electric) propulsion architecture simulation framework. A particular focus of the methodology was placed on the polarization curve modelling, which was designed to be pressure and temperature dependent, allowing for detailed assessments of FC operating behaviors.

The two FCS configurations were assessed based on a bottom-up approach. At the cell level, the impact of operating pressure on total system mass, mission fuel consumption and TMS drag was presented. Especially the reduction in operating pressure was found to result in a significant decrease in all three parameters. This was due to the fact that lower stack operating pressures require less cathode stream pressurization, which in turn leads to a reduction in the overall stack power requirements.

On the stack level different oversizing factors were evaluated. Large stack oversizing lead to increased FCS masses, but with reduced mission fuel masses and TMS drag. These counteracting

trends demonstrated a high potential for further FCS optimizations on an aircraft integrated level, as all three parameter outputs can have a significant impact on aircraft performance.

In order to analyze possible FC technology advancements, the impact of three different technology scenarios was assessed. Similarly to the oversizing study, the impact of FC specific powers will have to be closely monitored for aircraft integration and should be optimized during aircraft integration.

Finally, a brief study on the TMS was conducted in order to assess optimal stack coolant temperatures. For a maximum drag reduction, high coolant inlet and low coolant outlet temperatures were beneficial. Lowest masses were achieved for low to medium coolant temperature deltas. The trends for TMS mass and drag exhibited opposing trends, indicating the necessity for further optimization of the TMS to achieve a minimal impact on aircraft operation.

With regard to future work, the novel FC-APU and FC-APPU will have to be modelled in an aircraft integrated assessment in order to optimize the interactions between total FCS mass, mission fuel consumption and TMS drag. Additionally, varying FC operational behavior will have to be analyzed. These and further challenges will be assessed in future studies of the Horizon Europe project HOPE.

7. Funding

This research was co-funded by the European Union under the Horizon Europe Research and Innovation program Grant Agreement No. 101096275 and UKRI Research and Innovation (UKRI) under the UK government's Horizon Europe funding guarantee No. 10068673.

8. Contact Author Email Address

All correspondence regarding this paper should be addressed to: moritz.kolb@bauhaus-lufffahrt.net

9. Copyright Statement

The authors confirm that they, and/or their company or organization, hold copyright on all of the original material included in this paper. The authors also confirm that they have obtained permission, from the copyright holder of any third party material included in this paper, to publish it as part of their paper. The authors confirm that they give permission, or have obtained permission from the copyright holder of this paper, for the publication and distribution of this paper as part of the ICAS proceedings or as individual off-prints from the proceedings.

References

- [1] Air Transport Action Group. *Tracking aviation efficiency – Fact sheet #3*. Fact Sheet, Aviation: Benefits Beyond Borders, 2019.
- [2] Klöwer M, Allen M, Lee D, Proud S, Gallagher L, Agnieszka S. *Quantifying aviation's contribution to global warming*. ESS Open Archive, 2021, DOI: 10.1002/essoar.10507359.1.
- [3] European Environment Agency, European Union Aviation Safety Agency. *European aviation environmental report 2022*. Publications Office of the European Union, 2023, DOI: 10.2822/04357.
- [4] International Civil Aviation Organization. *Post-COVID-19 forecasts scenarios*. <https://www.icao.int/sustainability/Pages/Post-Covid-Forecasts-Scenarios.aspx> (accessed 6th of December 2023).
- [5] van der Sman E, Peerlings B, Kos J, Lieshout R, Boonekamp T. *Destination 2050 – A route to net zero European aviation*. Royal Netherlands Aerospace Centre, NLR-CR-2050-510, 2021.
- [6] Air Transport Action Group. *Waypoint 2050*. Report, Aviation: Benefits Beyond Borders, 2021.
- [7] Fan L, Tu Z, Chan S H. Recent development of hydrogen and fuel cell technologies: A review. *Energy Reports*, Vol. 7, pp 8421-8446, 2021, DOI: 10.1016/j.egy.2021.08.003.
- [8] Gittleman C S, Jia H, de Castro E S, Chisholm C R I, Kim, Y S. Proton conductors for heavy-duty vehicle fuel cells. *Joule*, Vol. 5, Issue 7, pp 1660-1677, 2021, DOI: 10.1016/j.joule.2021.05.016.
- [9] Haider R, Wen Y, Ma Z-F, Wilkinson D P, Zhang L, Yuan X, Song S, Zhang J. High temperature proton exchange membrane fuel cells: Progress in advanced materials and key technologies. *Chemical*

MODELLING AND INITIAL ASSESSMENT OF A FUEL CELL AUXILIARY PROPULSION AND POWER UNIT

Society Reviews, Vol. 50, Issue 2, pp 1138–1187, 2021, DOI: 10.1039/d0cs00296h.

- [10] Eelman S, del Pozo y de Poza I, Krieg T. Fuel cell APU's in commercial aircraft – An Assessment of SOFC and PEMFC concepts. *24th International Congress of the Aeronautical Sciences*, Yokohama, Japan, ICAS 2004-7.6.3, 2004.
- [11] Daggett D L, Eelman S, Kristiansson G. Fuel cell APU for commercial aircraft. *AIAA/ICAS International Air and Space Symposium and Exposition: The Next 100 Years*, Dayton, Ohio, AIAA 2003-2660, 2003, DOI: 10.2514/6.2003-2660.
- [12] Zaghari B, Zhou T, Enalou H B, Pontika E, Laskaridis P. The impact of multi-stack fuel cell configurations on electrical architecture for a zero emission regional aircraft. *AIAA SCITECH 2023 Forum*, National Harbour, MD & Online, AIAA 2023-1593, 2023, DOI: 10.2514/6.2023-1593.
- [13] European Commission, Community Research and Development Information Service, HOPE Consortium. *Hydrogen optimized multi-fuel propulsion system for clean and silent aircraft*. <https://cordis.europa.eu/project/id/101096275> (accessed 6th of December 2023), DOI: 10.3030/101096275.
- [14] Yin F, Rao A G, Martinez R M, Eker T, Heidebrecht A, Kolb M G, Seitz A, Zhao X, Lim L, Mazzei L, Ponza R, Benini E. Hydrogen-optimized multi-fuel propulsion system for clean and silent aircraft. *EASN Conference 2023*, Salerno, Italy, 2023.
- [15] Vratny P C, Kling U. The impact of electric aircraft taxiing. *Deutscher Luft- und Raumfahrtkongress 2018*, Friedrichshafen, Germany, ID: 480115, 2018.
- [16] Seitz A, Habermann A L, van Sluis M. Optimality considerations for propulsive fuselage power savings. *Proceedings of the Institution of Mechanical Engineers; Part G: Journal of Aerospace Engineering*, Vol. 235, Issue 1, pp 22-39, 2020, DOI: 10.1177/0954410020916319.
- [17] Lv P, Ragni D, Hartuc T, Veldhuis L, Rao A G, Experimental investigation of the flow mechanisms associated with a wake ingesting propulsor. *AIAA Journal*, Vol. 55, Issue 4, pp 1332–1342, 2017, DOI: 10.2514/1.J055292.
- [18] Della Corte B, van Sluis M, Veldhuis L, Rao A G. Power balance analysis experiments on an axisymmetric fuselage with an integrated boundary-layer-ingesting fan. *AIAA Journal*, Vol. 59, Issue 12, pp 5211-5224, 2021, DOI: 10.2514/1.J060570.
- [19] Seitz A, Nickl M, Troeltsch F, Ebner K. Initial assessment of a fuel cell-gas turbine hybrid propulsion concept. *Aerospace 2022*, Vol. 9, Issue 2, 2022, DOI: 10.3390/aerospace9020068.
- [20] Lüdemann M, Engelmann M, Kellermann H, Maas P, Peter F, Hornung M, Troeltsch F. BLADE: A modular environment for traceable and automated aircraft design. Presentation, *EASN Conference 2023*, Salerno, Italy, 2023.
- [21] Bijewitz J, Seitz A, Hornung M. Power plant pre-design exploration for a turbo-electric propulsive fuselage concept. *AIAA Propulsion and Power Forum 2018*, Cincinnati, Ohio, AIAA 2018-4402, 2018, DOI: 10.2514/6.2018-4402.
- [22] Kaiser S, Seitz A, Donnerhack S, Lundbladh A. Composite cycle engine concept with hectopressure ratio. *Journal of Propulsion and Power*, Vol. 32, Issue 6, 2026, DOI: 10.2514/1.B35976.
- [23] Seitz A, Nickl M, Stroh A, Vratny P C. Conceptual study of a mechanically integrated parallel hybrid electric turbofan. *Proceedings of the Institution of Mechanical Engineers, Part G: Journal of Aerospace Engineering*, Vol. 232, Issue 14, pp 2688-2712, 2018, DOI: 10.1177/0954410018790141.
- [24] Türkyilmaz B, Lüdemann M, Kolb M G, Lessis A. Definition of a short-to-medium range aircraft for entry into service in 2035. Presentation, *EASN Conference 2024*, Thessaloniki, Greece, 2024 (abstract submitted)
- [25] van Wensveen J, Peter F, Rau T, Hornung M. Assessment of a fuel cell powered full electric subsystem architecture for the AVACON research baseline aircraft. *Deutscher Luft- und Raumfahrt Kongress 2019*, Darmstadt, Germany, 2020. DOI: 10.25967/490114.
- [26] Chakraborty I. *Subsystem architecture sizing and analysis for aircraft conceptual design*. Dissertation, Daniel Guggenheim School of Aerospace Engineering, Georgia Institute of Technology, 2015.
- [27] Rao N K. *Influence of parametric modelling of wing subsystems on the aircraft design and performance*. Master's dissertation, Faculty of Aerospace Engineering, Delft University of Technology, 2017.
- [28] Daly M, Gunston B. *IHS Jane's Aero-Engines*. IHS Ltd, 2013.
- [29] Luo F, Zhang Q, Yang Z, Guo L, Yu X, Qu K, Ling Y, Yang J, Cai W. Fabrication of stable and well-connected proton path in catalyst layer for high temperature polymer electrolyte fuel cells. *ChemCatChem 2018*, Vol. 10, Issue 22, pp 5314–5322, 2018, DOI: 10.1002/cctc.201801256.
- [30] Choi S, Kucharczyk C J, Liang Y, Zhang X, Takeuchi I, Ji H-I, Haile S M. Exceptional power density and stability at intermediate temperatures in protonic ceramic fuel cells. *Nature Energy*, Vol. 3, pp 202–210, 2018, DOI: 10.1038/s41560-017-0085-9.
- [31] Scholta J, Messerschmidt M, Jörissen L, Hartnig Ch. Externally cooled high temperature polymer electrolyte membrane fuel cell stack. *Journal of Power Sources*, Vol. 190, Issue 1, pp 83-85, 2009, DOI:

MODELLING AND INITIAL ASSESSMENT OF A FUEL CELL AUXILIARY PROPULSION AND POWER UNIT

10.1016/j.jpowsour.2008.10.124.

- [32] Kellermann H, Lüdemann M, Pohl M, Hornung M. Design and optimization of ram air-based thermal management systems for hybrid-electric aircraft. *Aerospace 2021*, Vol. 8, Issue 1, 2020, DOI: 10.3390/aerospace8010003.
- [33] OpenMDAO. *Welcome to OpenMDAO*. <https://openmdao.org/newdocs/versions/latest/main.html> (accessed 24th of April 2024).
- [34] Larminie J, Dicks A. *Fuel cell systems explained*. 2nd Edition, John Wiley & Sons Ltd, 2003.
- [35] Newman J, Balsara N P. *Electrochemical systems*. 4th Edition, Wiley, 2021.
- [36] Spiegel C. *PEM fuel cell modelling and simulation using MATLAB*. Elsevier Inc., 2008.
- [37] International Civil Aviation Organization. *Manual of the ICAO standard atmosphere - extended to 80 kilometres / 262,500 feet (Doc 7488)*. 3rd Edition, ICAO, DOC-07488-003-01, 1993.
- [38] Tornabene R, Wang X-Y, Steffen C J, Freeh J E. Development of parametric mass and volume models for an aerospace SOFC/gas turbine hybrid system. NASA, NASA/TM-2005-213819, 2005.
- [39] Kellermann H. *Design of thermal management systems for future aircraft*. Dissertation, Technical University of Munich, Department of Aerospace and Geodesy, Institute of Aircraft Design, 2023.
- [40] EH Group. *EH fuel cell stacks*. Product Data Sheet, EH Group, 2023-A, 2023.
- [41] FlyZero. *Fuel cells roadmap report*. Report, FlyZero Aerospace Technology Institute, FZO-PPN-COM-0033, 2022.
- [42] HyPoint. *Hypoint technical white paper*. White Paper, HyPoint Inc., 2021.
- [43] Habermann A L, Kolb M G, Maas P, Kellermann H, Rischmüller C, Peter F, Seitz A. Study of a regional turboprop aircraft with electrically assisted turboshaft. *Aerospace 2023*, Vol. 10, Issue 6, 2023, DOI: 10.3390/aerospace10060529.
- [44] Hall D K, Greitzer E M, Dowdle A P, Gonzalez J J, Hoburg W W, Lang J H, Sabnis J S, Spakovsky Z S, Yutko B, Courtin C, Thalheimer W, Trollinger L, Tylko J, Varney N, Uranga A, Byahut S, Kruger M. *Feasibility of electrified propulsion for ultra-efficient commercial aircraft final report*. Report, NASA, NASA/CR-2019-220382, 2019.
- [45] Dynalene. *Dynalene HC series*. Product Data Sheet, Dynalene, 2020.
- [46] Bell I H, Wronski J, Quoilin S, Lemort V. Pure and pseudo-pure fluid thermophysical property evaluation and the open-Source thermophysical property library CoolProp. *Industrial & Engineering Chemistry Research 2014*, Vol. 53, Issue 6, pp 2498-2508, 2014, DOI: 10.1021/ie4033999.
- [47] Battiston A, Magrini A, Ponza R, Benini E, Türkyilmaz B, Seitz A, Heidebracht A. Design optimisation of a boundary layer ingestion propulsor. *34th International Congress of the Aeronautical Sciences*, Florenz, Italy, ICAS2024-2.3.2, 2024.
- [48] Seitz A, Habermann A L, Peter F, Troeltsch F, Pardo A C, Della Corte B, van Sluis M, Goraj Z, Kowalski M, Zhao X, Grönstedt T, Bijewitz J, Wortmann G. Proof of concept study for fuselage boundary layer ingesting propulsion. *Aerospace 2021*, Vol. 8, Issue 1, 2021, DOI: 10.3390/aerospace8010016.

Appendix A

Table A – Subsystem ATA chapters with corresponding modelling approaches

ATA	Name	Modelling approach
21	Air conditioning	Method based on Chakraborty [26]
22	Auto flight	Power scaled with MTOM
23	Communication	Power scaled with MTOM
24	Electrical power	Power scaled with MTOM
25	Equipment and furnishings	Power scaled with passenger number; full galley peak load at beginning of climb and middle of cruise
26	Fire protection	Power scaled with MTOM
27	Flight controls	Airbus A320 results of Rao [27] scaled with wing area and flight phase
28	Fuel	Power scaled with MTOM
30	Ice and rain protection	Power scaled with MTOM
31	Indicating and recording systems	Power scaled with MTOM
32	Landing gear	Power scaled with MTOM
33	Lights	Power scaled with MTOM
34	Navigation	Power scaled with MTOM
35	Oxygen	Power scaled with passenger number
38	Water and waste	Power scaled with passenger number
45	Central maintenance system	Power scaled with MTOM
46	Information system	Power scaled with MTOM
52	Doors	Power scaled with MTOM
73	Engine fuel and control	Power scaled with MTOM
74	Ignition	Power scaled with MTOM
76	Engine controls	Power scaled with MTOM
77	Engine indicating	Power scaled with MTOM
78	Exhaust	Method based on Chakraborty [26]
80	Starting / Relight	Boeing 787 starting power [28] scaled with maximum engine thrust